Iranian Journal of Basic Medical Sciences
ijbms.mums.ac.ir

MiR-124 alleviates cerebral ischemia-reperfusion injury by targeting SLC1A5 to inhibit neuronal ferroptosis

Yizhen Zhu [1#], Qian Jiang [2#], Tingting Long [2], Tao Huang [2], Junde Zhu [2*]

[1] Class 5, Grade 2023, Clinical Medicine, Guizhou Medical University, Gui'an New District, Guizhou 561113, People's Republic of China
[2] Department of Anatomy and Neurobiology, Guizhou Medical University School of Basic Medicine, Gui'an New District, Guizhou 561113, People's Republic of China

ARTICLE INFO

Article type:
Original

Article history:
Received: Dec 24, 2025
Accepted: Jun 15, 2026

Keywords:
Cerebral Ischemia
Ferroptosis
MiR-124
Neuroprotection
Reperfusion Injury
Solute carrier family 1 member 5

ABSTRACT

Objective(s): This study aimed to investigate whether miR-124 alleviates neurological injury in cerebral ischemia-reperfusion injury (CIRI) mice by targeting Solute Carrier Family 1 Member 5 (SLC1A5) to regulate ferroptosis.

Materials and Methods: One hundred twenty male C57BL/6 mice were randomly assigned to Sham, CIRI model, miR-124 mimic, miR-124 inhibitor, miR-124 vector, and Ferrostatin-1 (Fer-1) groups. One week before modeling, the viral groups received 2.0 μl of the corresponding viral vector via right lateral ventricle injection. Additionally, the Fer-1 group received intraperitoneal injections of ferrostatin-1 (5.0 mg/kg). Following the establishment of the MCAO model by the wire occlusion method. At different time points, the Longa method was employed to assess the degree of neurological deficit. TTC staining was used to detect cerebral infarction volume. ELISA was applied to measure changes in SOD, MDA, GSH, and Fe^{2+}. qRT-PCR was utilized to detect the expression levels of miR-124, SLC1A5, and GPX4, and Immunohistochemistry was detected SLC1A5-positive cells. Finally, the miR-124/SLC1A5 interaction was predicted by bioinformatics and validated by a dual-luciferase assay and western blot.

Results: Compared with the sham group, the CIRI group showed reduced neurological scores, elevated MDA/Fe^{2+}, and decreased SOD/GSH/GPX4. miR-124 mimic treatment significantly improved these parameters, similar to Fer-1, whereas miR-124 inhibition exacerbated injury and increased SLC1A5 expression. Dual-luciferase assay confirmed SLC1A5 as a direct target of miR-124.

Conclusion: Collectively, these data indicate that MiR-124 attenuates CIRI-induced neurological damage, potentially by targeting SLC1A5 to inhibit ferroptosis, as evidenced by up-regulation of GPX4 and GSH.

▶ Please cite this article as:
Zhu Y, Jiang Q, Long T, Huang T, Zhu J. MiR-124 alleviates cerebral ischemia-reperfusion injury by targeting SLC1A5 to inhibit neuronal ferroptosis. Iran J Basic Med Sci 2026; 29:

Introduction

In recent years, the incidence of ischemic stroke in China has exhibited a steadily increasing trend, positioning the country at the forefront of global statistics (1). CIRI represents a significant exacerbation of tissue damage occurring in regions that have been reperfused after an ischemic event. The underlying mechanisms contributing to this injury are primarily attributed to excessive free radical production (2), excitotoxicity from amino acids (3), mitochondrial dysfunction (4), and ferroptosis (5). Current primary treatments for ischemic stroke include intravenous thrombolysis (6) and surgical thrombectomy (7). However, widely used thrombolytic agents, such as recombinant tissue plasminogen activator (rt-PA) (8) and urokinase (9), carry an elevated risk of hemorrhagic transformation. Additionally, mechanical thrombectomy is limited by narrow therapeutic time windows and various contraindications (10), resulting in many patients being left without viable treatment options following a stroke. Consequently, identifying effective neuroprotective strategies and mitigating CIRI progression remain critical challenges in contemporary stroke management.

Research has demonstrated that Solute Carrier Family 1 Member 5 (SLC1A5) serves as a critical component of the amino acid transport system, exhibiting high affinity for glutamine and primarily mediating its transmembrane uptake (11). Accumulating evidence indicates that overexpression of SLC1A5 results in elevated intracellular glutamate levels (12). Elevated glutamate concentrations suppress ferroptosis by inhibiting the cystine/glutamate antiporter system (system xc−), which in turn down-regulates SLC1A5 expression (13). This regulatory feedback loop limits excessive conversion of glutamine to glutamate via mitochondrial glutaminase (14). Consequently, this mechanism enhances the activity of the cystine/glutamate exchanger, preserves cellular anti-oxidant capacity, and ultimately inhibits ferroptosis (15). However, the precise

*_Corresponding author:_ Junde Zhu. Department of Anatomy and Neurobiology, Guizhou Medical University School of Basic Medicine, Gui'an New District, Guizhou 561113, P.R.China. Tel: +86-851-88416251, Email: jdzhu73@126.com
#These authors contributed eqully to this work

molecular mechanisms underlying SLC1A5 regulation in this pathway remain poorly understood.

Extensive evidence suggests that microRNAs (miRNAs) play a crucial role in regulating the progression of ischemic brain injury by targeting and degrading specific mRNAs or inhibiting their translation, thereby controlling gene expression at the transcriptional level (16). Notably, clinical studies have demonstrated that stroke patients exhibit significantly reduced levels of miR-124 in their bloodstream; conversely, elevated miR-124 levels have been linked to enhanced post-injury brain repair (17). Prior investigations by our group confirmed a marked decrease in miR-124 expression in brain tissue from mouse models subjected to CIRI (18, 19). Furthermore, our findings indicate that pharmacologically increasing miR-124 expression can ameliorate neurological deficits in these models, potentially by modulating mitochondrial autophagy (19). Recent cellular studies have confirmed the relationship between miR-124 and its target, SLC1A5 (20). Recent cellular studies have underscored the interaction between miR-124 and its target, SLC1A5, revealing that increased miR-124 levels suppress ferroptosis, whereas decreased levels promote it (21). Despite these insights, there is a paucity of reports, both domestically and internationally, examining whether targeting SLC1A5 with miR-124 affects neuronal ferroptosis following CIRI. Thus, the present study aims to utilize a mouse model of middle cerebral artery occlusion (MCAO) to delineate the relationship between miR-124 overexpression/knockdown, SLC1A5, and ferroptosis. Our objective is to uncover novel therapeutic targets and provide experimental evidence that could inform the prevention and treatment of ischemic stroke in clinical practice.

Materials and Methods

Main reagents

MCAO suture (Shanghai Saibai Kang Biotechnology Co., Ltd., China, catalog 2436); miR-124 mimic and miR-124 inhibitor/vector (Gema Gene Co., Ltd. China); Trizol Reagent RNA Kit (Invitrogen, USA, catalog 264909); Ferrostatin-1 assay kit (Invitrogen, USA, catalog BW275B); Western blot secondary antibody and primary antibody diluent (Biosharp, USA, catalog BL543A, BL517A); High-Efficiency Radioimmunoprecipitation Tissue/Cell Rapid Lysis Buffer (Nanjing Jiancheng Engineering Research Institute, China, catalog F3547); Anti-GAPDH Rabbit Polyclonal Antibody (Invitrogen, USA, catalog BL006B). The electrochemiluminescence (ECL) substrate kit (Wuhan Sanying Biotechnology Co., Ltd., China, catalog BL520A) was utilized in conjunction with the superoxide dismutase (SOD), malondialdehyde (MDA) (Shenyang Wanlei Biotechnology Co., Ltd., China, catalog BC1286, BC1252), and the SLC1A5 antibody (Cat: K004913P), glutathione peroxidase 4 (GPX4) antibody, reduced glutathione (GSH) assay kit, and iron assay kit (APExBIO, USA, catalog K003083P, BC1175, B26465).

Main instruments and equipment

Stereotaxic instrument (Shenzhen Ruowei Company, China); ultra-sensitive, fully automated chemiluminescence analyzer (Proteinsimple, Germany); S25 electric glass homogenizer (Proteinsimple, Germany); microscope (DP73, Olympus, Japan); rotary microtome (Proteinsimple, Germany); HM-200 electronic balance (Guangdong Tianpu Biochemical Pharmaceutical Co., Ltd., China); LightCycler 96 instrument PCR system (Malvern Instruments Ltd., UK); L-15K high-speed refrigerated centrifuge (IKA GmbH, Germany); MDF-382E ultra-low temperature freezer (Sanyo Electric Co., Ltd., Japan).

Experimental animals

One hundred twenty healthy male SPF-grade C57BL/6 mice, aged three months and weighing 20±0.5 g, were provided by the Guizhou Medical University (GMU) Laboratory Animal Center for this study (Animal license number: SYXK(Gui)2025-0001). The mice were individually housed in cages under controlled environmental conditions at the GMU Laboratory Animal Center, maintaining an ambient temperature of 20–25 °C, relative humidity of 50–60%, and a 12-hr light-dark cycle. The animals were given *ad libitum* access to water and food. This study received approval from the GMU Animal Ethics Committee (Approval No. 2500122), and all experimental procedures and animal handling complied with the Regulations on the Management of Animal Experiments.

MCAO model and grouping

A mouse model of middle cerebral artery occlusion (MCAO) was established using a modified Zea-Longa ligation technique (22). The sham surgery group underwent only a midline cervical incision without any ligation of the middle cerebral artery. According to the neurological deficit scoring system developed by Longa *et al.* (23), successful modeling criteria were met when the mice were awake postoperatively but unable to walk in a straight line, exhibiting right-sided hemiplegia and receiving a neurological score ranging from 1 to 3. Following this, the mice were randomly divided into six groups (n=20): Sham group, Model (CIRI) group, miR-124 mimic group, miR-124 inhibitor group, miR-124 vector group, and Ferrostatin-1 (Fer-1) ferroptosis inhibitor group.

Adeno-associated virus injection into the lateral ventricle

Administer 1.0 % sodium pentobarbital (50 mg/kg) via intraperitoneal injection to anesthetize mice, then secure them in a stereotaxic brain mount. Aspirate 2.0 µl of purified adeno-associated virus (AAV) solution successfully constructed by our research group (18). Position the syringe tip at the midbrain artery marker and drill the following coordinates: Y-axis AP: 0, X-axis ML: -1.5 mm, Y-axis DV: -2.5 mm (relative to the anterior fontanelle and dura mater surface). After reaching a needle depth of 2.5 mm, slowly inject the AAV miR-124 mimic, miR-124 inhibitor, or empty vector. Additionally, mice in the Fer-1 group received an intraperitoneal injection of the ferroptosis inhibitor (5.0 mg/kg). The MCAO/R model was established one week later.

Neurologic deficit score

The Longa scoring system was used to assess neurological damage in mice at different time points following cerebral reperfusion (23). The scoring criteria are as follows: 0 points, No neurological deficits with normal activity; 1 point, Inability to extend the contralateral forelimb fully; 2 points, Circular crawling with tail-chasing behavior; 3 points, Body leaning toward the paralyzed side; 4 points, Inability to walk spontaneously with loss of consciousness.

TTC staining

Mice were euthanized by intraperitoneal injection of 1%

sodium pentobarbital. Brains were rapidly removed and frozen at -20 °C for 20 min, then thawed on ice for 3 min. Next, remove the olfactory bulb and cerebellum, then section the brain into slices approximately 2.0 mm thick. Transfer these slices to a 2.0% solution of 2,3,5-Trichlorotriphenyltetrazole (TTC) staining solution and incubate them at 37 °C in the dark for 25 min. After incubation, wash away any excess stain using a tissue wash buffer. Fix the samples in a 4% paraformaldehyde solution and store them overnight at 4 °C. After 24 hr, capture images using a high-definition smartphone. Measure the area of brain tissue across all sections with Image Pro Plus version 9.0 software (Media Cybernetics, USA).

ELISA detection

To prepare a 10% rat brain homogenate, utilize a tissue homogenizer set to 10,000–15,000 rpm for 10 sec per cycle. Allow a 30-second pause between cycles, and repeat this process for 3–5 iterations. Following homogenization, centrifuge the resulting mixture at 2,500 rpm for 10 min at 4 °C. Carefully collect the supernatant for subsequent analysis. Employ the specified kit protocols to quantitatively assess the levels of superoxide dismutase (SOD), malondialdehyde (MDA), and glutathione (GSH) in the rat brain tissue.

Fe^{2+} content determination

Begin by taking 10.0 mg of ischemic brain tissue and washing it with pre-chilled phosphate-buffered saline (PBS) to remove any residual contaminants. Subsequently, add 10 volumes of iron detection buffer and homogenize the tissue on ice for a total of 15 cycles. Following homogenization, centrifuge the mixture at 12,000 RPM for 10 min to separate the cellular components. Carefully transfer the resulting supernatant to a plastic centrifuge tube for future analysis. Assess the concentration of Fe^{2+} in the sample by following the detailed instructions provided with the detection kit.

qRT-PCR assays

After homogenizing the tissues, total RNA was extracted according to the RNA extraction kit instructions, followed by reverse transcription. Next, we established the PCR system and cycled through denaturation, annealing, and extension steps. After completing the PCR, melting curve analysis was performed on the products at 95 °C (15 s) and 60 °C (30 sec). The software automatically analyzes and plots the melting curves of PCR products to determine PCR specificity. Real-time quantitative PCR data analysis: The built-in analysis software of the fully automated real-time fluorescent quantitative PCR system was employed to process PCR data using a two-step method. Each sample was subjected to triplicate experiments. Primer sequences are listed in Table 1. U6 and GAPDH served as the internal reference genes. The relative expression levels of the target genes were determined using the $2^{-\Delta\Delta Ct}$ method.

Immunohistochemical detection

The brain tissue blocks were removed and stored overnight at 4 °C. They were dehydrated with 20% and 30% sucrose solutions, then sectioned at 10 μm thickness using a cryostat. The sections were incubated with Solution A for 10 min following the kit instructions, washed with PBS three times for 5 min each, then treated with Solution B for 10 min. After removing Solution B, the sections were incubated with SLC1A5 monoclonal antibody (diluted 1:150) for 2 hr, followed by three 5-min washes with PBS. Subsequently, Solution C was applied for 10 min, then washed three times with PBS. Solution D was added and incubated for 10 min, with subsequent washes. DAB chromogenic solution was used for staining, followed by rinsing with running water. The sections were counterstained with hematoxylin for 1 min, then rinsed to remove excess stain, differentiated briefly for 15 sec, rinsed again and counterstained with blue for 30 sec before a final rinse. The samples were dehydrated in absolute ethanol for 2 min, cleared in xylene for 2 min, and mounted with neutral binder. For analysis, five non-overlapping fields per slide were randomly selected and measured using ImageJ software.

Table 1. Primer sequences of studied neuronal ferroptosis and reference genes in qRT-PCR analysis

gene	Primer sequence (5' → 3')
miR-124	CGCGCGTTATTGCTTAAGAA
	AGTGCGGGTTCCGAGGTATT
SLC1A5	CCCGGATCTACACCACCTGA
	AACTGGGAGTTGAGAGAGCC
GPX4	CATTCCCGAGCCTTTCAACC
	CACACGCAACCCCTGTACTT
U6	GTCCTCGTTGCTCGTTGCTCG
	CTCGCTTCGGCAGCACATAT
GAPDH	CTCTCTGCTCCTCCCTGTTC
	TCACACCGACCTTCACCATC

Database prediction and dual luciferase reporter analysis

We identified potential target genes for miR-124 using the TargetScan, PicTar, and miRWalk databases and selected the intersection of these databases. Next, the sequence containing the miR-124 binding site in the SLC1A5 3′UTR was amplified and cloned into the pGL3-basic luciferase plasmid to create the wild-type SLC1A5 (SLC1A5-WT) recombinant plasmid. The miR-124 binding site on SLC1A5-WT was mutated using a point mutation kit to construct a mutant SLC1A5 (SLC1A5-MUT) recombinant plasmid. Cultured 293T cells were seeded in 24-well plates. Once the cells reached 85% confluence, SLC1A5-WT or SLC1A5-MUT reporter plasmids were co-transfected with either miR-124, the negative control (miR-NC), anti-miR-124, or anti-miR-NC. Forty-eight hours later, the luciferase activity of the SLC1A5-WT or SLC1A5-MUT reporter plasmids was detected using the Dual-Luciferase® Reporter Assay System.

Western blotting assay

Brain tissue was collected from each group, and total protein was extracted. Protein concentration was determined using the Bicinchoninic acid (BCA) protein detection method. Proteins were separated by 10% SDS-PAGE and transferred to polyvinylidene fluoride (PVDF) membranes. The membranes were blocked overnight at 4 °C with 5% skimmed milk powder. The membranes were incubated with SLC1A5 and β-actin antibodies at 37 °C for two hours. The membranes were washed three times with phosphate-buffered Tween solution (PBST), incubated with the corresponding secondary antibody, and developed using an ECL reagent. ImageJ was used to analyze the relative expression levels of SLC1A5 in each cell group.

Statistical analysis

All data were presented as mean±standard deviation. Statistical analysis was performed using GraphPad Prism 9.0

(GraphPad Software, Inc., San Diego, CA, USA) to compare multiple groups. One-way or two-way analysis of variance (ANOVA) was performed, followed by Tukey's post hoc test for pairwise comparisons. All experiments were repeated at least three times to ensure reproducibility. $P<0.05$ indicates a statistically significant difference.

Results

Comparison of neurological deficit scores

To clarify the effect of miR-124 on cerebral ischemic injury in mice in this study, we first evaluated neurological deficits across groups at the same time point, as shown in Figure 1A. At 1, 3, 7, and 14 days after surgery, the neurological functional impairment scores of mice in the Sham group were all 0. The neurological deficit scores of the CIRI group were significantly higher than those of the sham group at all time points ($P<0.001$). The miR-124 mimic group showed significantly lower neurological deficit scores than the CIRI group at the corresponding time points ($P<0.01$). The miR-124 inhibitor and miR-124 vector groups showed significantly higher neurological deficit scores than the miR-124 mimic group ($P<0.05$). However, no statistically significant differences were observed between the miR-124 mimic and the Fer-1 groups in the aforementioned indicators ($P>0.05$). We again evaluated the neurological functional impairment of mice in each group at different time points, as shown in Figure 1B. Among them, the changes in the CIRI group, the miR-124 inhibitor group, and the miR-124 vector group were basically consistent. At the same time, the changes in the miR-124 mimic group and the Fer-1 group were also largely consistent, and both were most significant at 3 days, which might be an important intervention time point.

Comparison of cerebral infarct volume

TTC staining demonstrated that normal mouse brain tissue exhibited a red coloration, whereas infarcted tissue appeared white (Figure 1C). The cerebral infarction ratio was significantly higher in all experimental groups than in the Sham group ($P<0.001$). Notably, the cerebral infarction ratio was substantially reduced in the miR-124 mimic group relative to the CIRI group ($P<0.01$). The cerebral infarction ratios in the miR-124 inhibitor and miR-124 vector groups were intermediate between those of the Sham and miR-124 mimic groups ($P<0.05$). However, the difference in cerebral infarction ratio between the miR-124 mimic group and the Fer-1 group did not reach statistical significance ($P>0.05$; Figure 1D).

Comparison of Fe^{2+} and oxidative stress factor content

In comparison to the sham group, the CIRI group exhibited significantly elevated levels of MDA and Fe^{2+} in brain tissue, while SOD and GSH levels were markedly reduced ($P<0.001$). The brain tissue of the miR-124 mimic group demonstrated significantly decreased levels of MDA and Fe^{2+} and substantially increased levels of SOD and GSH relative to the CIRI group ($P<0.01$). In contrast, the miR-124 inhibitor and vector groups showed significantly higher levels of MDA and Fe^{2+} and significantly lower levels of SOD and GSH in brain tissue compared with the miR-124 mimic group ($P<0.05$). However, no statistically significant differences were observed between the miR-124 mimic group and the Fer-1 group in these indicators ($P>0.05$; Figure 1E).

Comparison of miR-124 expression levels with SLC1A5 and GPX4

Compared with the sham group, the CIRI group exhibited significantly reduced levels of miR-124 and GPX4

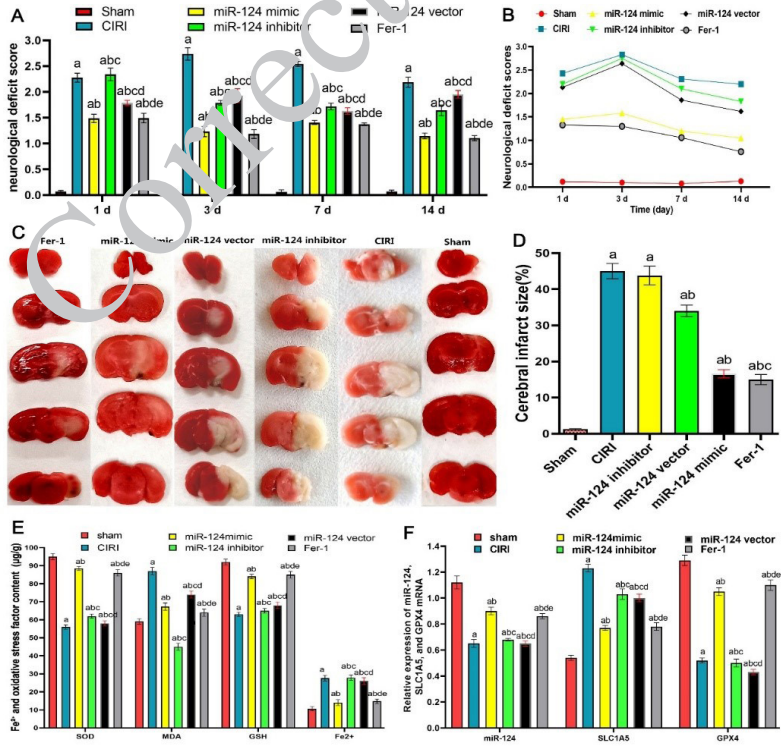

Figure 1. Effects of miR-124 on neuronal function, cerebral infarct volume, oxidative stress, and ferroptosis in mice

A. Comparison of neurological function defect scores among different groups at the same time point (n=20); B. Comparison of neurological function defect scores at different time points within the same group (n=20); C. Representative Images of Cerebral Infarct Area by TTC Staining; D. Percentages of brain infarct area in the ipsilateral hemisphere (n = 5); E. Quantification of Fe^{2+} and oxidative stress markers (n=5); F. Relative expression of miR-124, SLC1A5, and GPX4 mRNA. a$P<0.001$, compared with the sham group; b$P<0.01$, compared with the CIRI group; C$P<0.05$, compared with miR-124 mimic group; d$P<0.05$, compared with miR-124 inhibitor group; e$P<0.05$, compared with miR-124 vector group.

mRNA in ischemic brain tissue, while SLC1A5 mRNA expression was notably elevated (P<0.001). In the miR-124 mimic group, both miR-124 and GPX4 mRNA expression levels were significantly increased relative to those in the CIRI group, whereas SLC1A5 mRNA expression was substantially decreased (P<0.01). The miR-124 inhibitor and miR-124 vector groups demonstrated significantly lower levels of both miR-124 and GPX4 mRNA in ischemic brain tissue, accompanied by elevated SLC1A5 mRNA expression, compared with the miR-124 mimic group (P<0.05). However, no statistically significant differences were detected between the miR-124 mimic and Fer-1 groups in the aforementioned indicators (P>0.05; Figure 1F).

Comparison of SLC1A5-positive cell counts

The number of SLC1A5-positive cells in the CA1 region of the hippocampus in the CIRI mice was significantly higher than that in the sham group (P<0.001). In contrast, the number of SLC1A5-positive cells in the hippocampus of miR-124 mimic mice was notably lower than that in the CIRI group (P<0.01). Furthermore, the number of SLC1A5-positive cells in the hippocampal CA1 region of mice in the miR-124 inhibitor and miR-124 vector groups was significantly higher than that in the miR-124 mimic group (P <0.05). However, the difference in the number of SLC1A5-positive cells between the miR-124 mimic and Fer-1 groups was not statistically significant (Figures 2A and 2B).

Potential target analysis and validation

A nucleotide sequence complementary to miR-124 was identified at positions 1302–1310 within the SLC1A5 3′UTR region using TargetScan software prediction (Figure 2C). A dual luciferase reporter assay demonstrated that, in comparison to the miR-NC group, the luciferase activity of SLC1A5-WT was significantly inhibited by miR-124 overexpression (0.97±0.05 vs. 0.35±0.03, t=12.673, P<0.05). In contrast, the luciferase activity of SLC1A5-MUT remained unaffected (P>0.05). Similarly, relative to the anti-miR-NC group, inhibition of miR-124 significantly increased the luciferase activity of SLC1A5-WT (1.15± 0.07 vs. 3.67±0.32, t=12.304, P<0.05), while exerting no effect on SLC1A5-MUT luciferase activity (P>0.05). These findings suggest that miR-124 can bind to SLC1A5 as a target. Western blotting results (Figure 2D) indicated that, compared with the miR-NC group, miR-124 overexpression significantly suppressed SLC1A5 protein expression (0.95± 0.06 vs. 0.24±0.01, t=8.385, P<0.05). Conversely, compared with the anti-miR-NC group, miR-124 overexpression markedly promoted SLC1A5 protein expression (0.24±0.01 vs. 2.57±0.26, t=12.216, P<0.05). These results demonstrate that SLC1A5 is highly expressed in cells and that miR-124 negatively regulates SLC1A5 protein expression.

Discussion

Cerebral ischemia-reperfusion is considered an effective therapeutic approach for improving the outcomes of acute ischemic stroke. However, after the blood supply is restored, brain tissue damage worsens due to pathological changes, such as ferroptosis. Ferroptosis is a recently identified form of cell death (24). Impaired clearance of reactive oxygen species (ROS) occurs when there is abnormal SLC1A5 expression (25), reduced GSH production, decreased GPX4 activity, and down-regulated anti-oxidant expression levels (25, 26). This leads to the accumulation of harmful lipid ROS, which damage cellular structure and function, ultimately resulting in cell death (26). This study found that, compared with the control group, the CIRI group exhibited elevated neurological deficit scores, MDA levels, Fe^{2+} content, and SLC1A5 expression, while SOD and GSH content, as well as GPX4 expression, were reduced. These results suggest that CIRI mice experienced ferroptosis due to disruption of

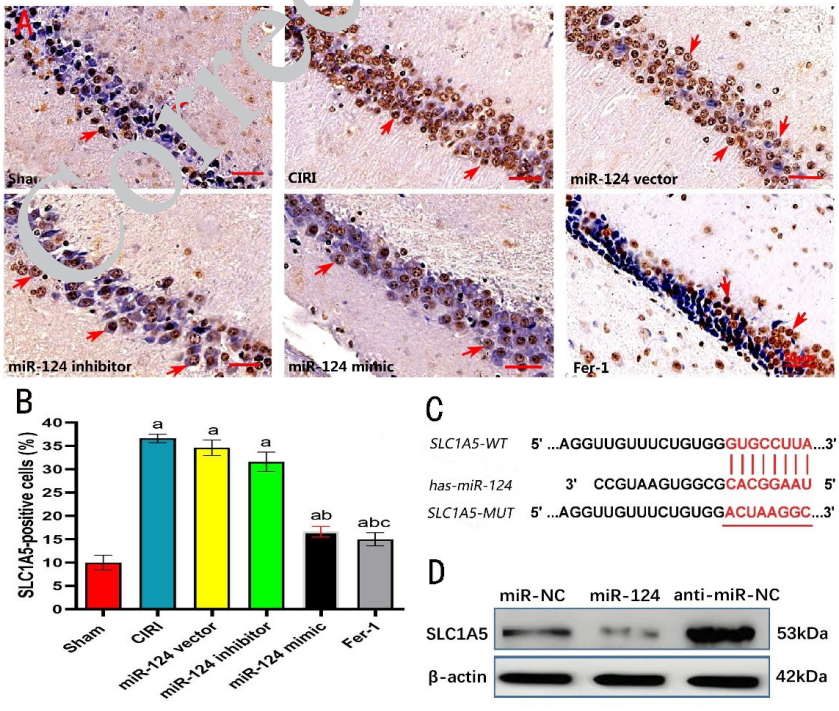

Figure 2. Analysis and validation of SLC1A5-positive cell expression in the mouse hippocampal CA1 region and Identification of miR-124 targets
A. Representative image of SLC1A5-positive cell expression in the mouse hippocampal CA1 region (red arrow); B. Comparison of SLC1A5-positive cell counts (n=5); C. Targeting sites between miR-124 and SLC1A5; D. Western blotting validates the function of the miR-124 target gene, SLC1A5 (n=5). aP<0.05, compared with the sham group; bP<0.01, compared with the CIRI group; cP<0.05, compared with miR-124 inhibitor group and miR-124 vector group.

the anti-oxidant system, imbalance of iron metabolism, and accelerated lipid peroxidation in brain tissue.

MicroRNAs (miRNAs) are non-coding RNAs, typically ranging from 18 to 22 nucleotides in length (27). Their primary function involves recognizing sequences within the 3' untranslated region (UTR) of target mRNA molecules. Upon binding to a specific sequence, miRNAs inhibit mRNA transcription and translation, thereby regulating the production of target proteins (28). Currently, miRNAs are recognized for their crucial regulatory roles in various diseases. miRNA-124, a novel miRNA, was initially identified in neural tissues and has been shown to inhibit stroke progression (29); however, the underlying mechanism remains unclear. Studies indicate that miRNAs can mitigate oxidative stress-induced injury caused by cerebral ischemia-reperfusion by regulating SLC1A5 (30). Other reports suggest that miR-124 mediates ferroptosis via the 3' UTR sequence of target mRNA, thereby suppressing oxidative stress damage (20). However, it remains unclear whether miR-124 acts via SLC1A5 to modulate oxidative stress and ferroptosis following CIRI. Therefore, investigating the regulatory mechanisms of ferroptosis following CIRI is a promising strategy for reversing neuronal damage in ischemic stroke.

Research has demonstrated that ischemic stroke initiates excitotoxic responses in brain tissue(31). These responses result in diminished GSH and GPX4 production within cells, alongside increased MDA levels (32). GSH is an intracellular anti-oxidant enzyme that scavenges oxygen-free radicals, and its levels serve as an indirect measure of cellular anti-oxidant capacity (33). MDA levels, on the other hand, reflect the extent of cellular damage caused by free radicals (32). A further significant contributor to ferroptosis is the elevated concentration of intracellular Fe^{2+}, which leads to enhanced lipid peroxidation and ROS production (34). Fer-1 acts as a selective inhibitor of erastin-induced ferroptosis (35), and it has been verified to augment anti-oxidant capacity and inhibit ferroptosis by obstructing cystine transport and glutathione production (36). The findings of this study revealed that the brain tissue of the miR-124 mimic group exhibited reduced MDA levels and SLC1A5 expression, while SOD and GSH levels increased. Conversely, the miR-124 inhibitor and vector groups displayed opposite changes in SOD, GSH, and MDA levels, as well as SLC1A5 expression in brain tissue. This suggests that miR-124 may exert anti-oxidant effects through SLC1A5, thereby further reducing ferroptosis.

Since Fe^{2+} is essential for the induction of ferroptosis, we investigated changes in divalent iron ions (Fe^{2+}) and the ferroptosis marker GPX4 in brain tissue to explore further whether miR-124 exerts anti-oxidant effects and mitigates ferroptosis via SLC1A5. The synthesis of GSH, a cofactor necessary for GPX4 function, is diminished, leading to reduced GPX4-mediated anti-oxidant activity and the onset or exacerbation of cellular ferroptosis (37). Consequently, GPX4 is a critical indicator of ferroptosis severity. However, the efficiency of GSH synthesis is constrained by the concentration of its substrate, cysteine, which is linked to the reverse transport mechanism mediated by the cystine/glutamate antiporter (38). Animal studies have demonstrated that immediate administration of the ferroptosis inhibitor Ferrostatin-1 (Fer-1) following CIRI in mice significantly alleviates neuronal damage and functional deficits following middle cerebral artery occlusion (35). This finding suggests that exogenous ferroptosis inhibitors may have potential therapeutic effects against CIRI. SLC1A5 functions as a transmembrane glycoprotein primarily responsible for transporting intracellular iron ions to extracellular spaces (13), and it has been recognized as a key iron transporter (37). Furthermore, SLC1A5 expression levels are closely associated with iron metabolism during ferroptotic events (15). Research indicates that ischemic stroke triggers excitotoxic reactions in brain tissue, leading to elevated intracellular Fe^{2+} levels and reduced GPX4 expression (39). Our study also revealed that Fer-1 significantly reduced Fe^{2+} concentrations and down-regulated SLC1A5 expression; concurrently, it upregulated superoxide dismutase (SOD), GSH content, and GPX4 expression. These alterations were largely consistent with those observed in the miR-124 mimic group. Based on these findings, we infer that miR-124 may target SLC1A5 to alleviate brain injury.

Conclusion

MiR-124 demonstrates neuroprotective effect in CIRI mice by targeting and modulating SLC1A5 and its associated proteins, thereby inhibiting ferroptosis. However, the presence of additional functional targets of miR-124 beyond SLC1A5 in the context of ferroptosis necessitates further investigation and validation. The authors have reviewed and approved the final version of the manuscript.

Acknowledgment

This research was part of a bachelor's thesis completed by Yizhen Zhu at Guizhou Medical University. The authors sincerely thank Dr Wenpeng Cao, Dr Yanqiao Ma, and Ms. Lingling Fu for their invaluable assistance with tissue slide preparation and biochemical analysis, respectively. The authors have no conflicts of interest regarding the publication of this article.

Ethical Approval

The animal ethics committee of the Guizhou Medical University (Guiyang, China) approved the entire experimental work (No. 2500122).

Funding

This work was supported by Guizhou Provincial Science and Technology Projects (Qiankehejichu-ZK- [2023] yiban 323), the Guizhou Medical University National Natural Science Foundation Cultivation Project (24NSFCP02), the Guizhou Provincial College Student Innovation and Entrepreneurship Project (2024106600537, x2024049), and the Science Innovation 2030—Brain Science and Brain Intelligence Technology Major Project (2021ZD0201100, 2021ZD0201103).

Authors' Contributions

Y Z and J Z conceived the research; Q J, T L, and T H performed the experiments; Q J analyzed the data; J Z and T H contributed reagents/materials/analysis tools; Y Z wrote the paper. All authors contributed to the discussion and revision of the manuscript.

Conflicts of Interest

All contributing authors declare no conflicts of interest regarding the publication of this paper.

Declaration

We acknowledge the use of ChatGPT (OpenAI, 2026) for grammar checking and to improve the manuscript's fluency.

References

1. Hu SY, Lei ZH, Wang Y, Ren LJ. Awareness of risk factors for cerebrovascular diseases among acute ischemic stroke patients in Shenzhen, China. Neurol Res 2024; 46:1046-1053.
2. Grzywna E, Stachura K, Moskala M, Kruczala K. Blood free radicals concentration determined by electron paramagnetic resonance spectroscopy and delayed cerebral ischemia occurrence in patients with aneurysmal subarachnoid hemorrhage. Cell Biochem Biophys 2017; 75:351-358.
3. Ruan LY, Wang ZN, Zheng MY, Zheng Q, Qing Q, Lin HY, *et al.* Polygoni *Multiflori Radix Praeparata* polysaccharides enhance gut health and mitigate ischemic stroke by regulating SCFA and amino acid metabolism in gut microbiota. Front Pharmacol 2025; 16:1580055.
4. Andrabi SS, Tabassum H, Parveen S, Parvez S. Ropinirole induces neuroprotection following reperfusion-promoted mitochondrial dysfunction after focal cerebral ischemia in Wistar rats. Neurotoxicology 2020; 77:94-104.
5. Chen W, Zhou X, Meng MY, Pan XR, Huang LY, Chen CX. Hyperbaric oxygen improves cerebral ischemia-reperfusion injury in rats via inhibition of ferroptosis. J Stroke Cerebrovasc Dis 2023; 32:107395.
6. KharismaTEA, Amalia L, Apriani L, Huda F, Cahyani A. Impact of pre-hospital and in-hospital optimization on the management of intravenous thrombolysis in hyperacute ischemic stroke: A scoping review. Risk Manag Healthc Policy 2025; 18:3689-3712.
7. Elgharabawi A, Moawad MHE, Wagih RM, Ahmed Y, Elkholy M, Serag I, *et al.* To bridge or not to bridge? A meta-analysis of intravenous thrombolysis before thrombectomy in large ischemic core strokes. Brain and Behavior 2025; 15: e71052.
8. Kaburagi K, Shimizu T, Hagiwara Y, Fukano T, Shibata S, Hoshino M, *et al.* Usefulness of carotid duplex ultrasonography in predicting residual large-vessel occlusions after intravenous recombinant tissue plasminogen activator therapy in patients with acute ischemic stroke. J Med Ultrason (2001) 2023; 50:103-109.
9. Hashmi TM, Shafiq A, Zia R, Ashraf H, Burhan M, Ahmed M, *et al.* Recombinant human pro-urokinase vs. alteplase within 4.5 hours of acute ischemic stroke: A systematic review and meta-analysis of randomized controlled trials. J Stroke Cerebrovasc Dis 2025; 34:108392.
10. Salsano G, Del Sette B, Bruzzone M, Mavilio N, Sassos D, Murialdo A, *et al.* Mechanical thrombectomy versus best medical treatment for patients with acute ischemic stroke and primary distal medium vessel occlusion: A systematic review and meta-analysis. Clin Neuroradiol 2026; 36:285-293.
11. Osman I, He XQ, Liu JH, Dong KZ, Wen T, Zhang FZ, *et al.* TEAD1 (Tea domain transcription factor 1) promotes smooth muscle cell proliferation through upregulating SLC1A5 (solute carrier family 1 member 5)-mediated glutamine uptake. Cir Res 2019; 124:1309-1322.
12. Wang YS, Wu JY, Zhang GC, Shi Y, Meng YC, Lv PP, *et al.* Androgens drive SLC1A5-dependent metabolic reprogramming in polycystic ovary syndrome. Nat Commun 2025; 16:7611.
13. Alfarsi LH, Ansari RE, Erkan B, Fakroun A, Craze ML, Aleskandarany MA, *et al.* SLC1A5 is a key regulator of glutamine metabolism and a prognostic marker for aggressive luminal breast cancer. Sci Rep 2025; 15:2805.
14. Duan YH, Peng S, Yue JN, Ding F, Chen XL, Pan WQ, *et al.* SLC1A5-dependent glutamine uptake in hepatocytes promotes liver regeneration. Hepatol Commun 2025; 9:e0742.
15. Wang D, Li L, Zhang F, Liu Q, Wang WL, Wang ZX, *et al.* SLC1A5 mediates myocardial damage after myocardial infarction by triggering cardiomyocyte ferroptosis. Biochemical Pharmacology 2025; 239.
16. Grigolashvili M, Kadyrova I, Shayakhmetova Y, Beisembayeva M, Muratbekova S, Koshelyuk A. Circulating microRNAs in various etiopathogenetic subtypes of acute ischemic stroke: a human systematic review study. Front Neurol 2025; 16:1623597.
17. Qi Z, Zhao YY, Su Y, Cao B, Yang JJ, Xing QH. Serum extracellular vesicle-derived miR-124-3p as a diagnostic and predictive marker for early-stage acute ischemic stroke. Front Mol Biosci 2021; 8:685088.
18. Zhu YZ, Zhao X, Liu RJ, Yang D, Ge G. Effect of oxygen-glucose deprivation of microglia-derived exosomes on hippocampal neurons: A study on miR-124 and inflammatory cytokines. J Mol Histol 2024; 55:349-357.
19. Zhu Y, Zou WJ, Sun BH, Shen K, Xia FY, Wang H, *et al.* Ginsenoside Rg1 regulates the activation of astrocytes through lncRNA-Malat1/miR-124-3p/Lamc1 axis driving PI3K/AKT signaling pathway, promoting the repair of spinal cord injury. CNS Neurosci Ther 2024; 30:e70103.
20. Bao WD, Zhou XT, Zhou LT, Wang FD, Yin XP, Lu YM, *et al.* Targeting miR-124/ferroportin signaling ameliorated neuronal cell death through inhibiting apoptosis and ferroptosis in aged intracerebral hemorrhage murine model. Aging Cell 2020;19:e13235.
21. Wu LL, Tian X, Zuo HW, Zheng WP, Li X, Yuan MS, *et al.* MiR-124-3p delivered by exosomes from heme oxygenase-1 modified bone marrow mesenchymal stem cells inhibits ferroptosis to attenuate ischemia-reperfusion injury in steatotic grafts. J Nanobiotechnology 2022; 20:196.
22. Plascencia M, Methner C, Kaul S. Pharmacological inhibition of GPR39 markedly reduces brain infarction in a mouse model of middle cerebral artery occlusion. Circulation 2025; 152:4357636.
23. Lim C, Kim H, Kim S, Kim HE, Moon SJ, Kim HH, *et al.* Assessing the effects of aging on the Koizumi's and Zea Longa's methods and their suitability as mouse models for evaluating neurodegeneration post-ischemic stroke: A comparative study. J Cereb Blood Flow Metab 2025; 45:2189-2202.
24. Tschuck J, Shafar V, Angeli JPF, Hadian K. The metabolic code of ferroptosis: nutritional regulators of cell death. Trends Biochem Sci 2025; 50:663-676.
25. Schneider N, Seitz R, Brandl N, Müller M, Gülow K. Reactive oxygen species across death pathways: gatekeepers of apoptosis, ferroptosis, pyroptosis, paraptosis, and beyond. Int J Mol Sci 2025; 26:10240.
26. Park SY, Ryu MH, Kim W, Garcia-Godoy F, Kwon YH, Jang HO. Reactive oxygen species-mediated oral cancer cells treatment using photosensitizer-combined carbon dots via apoptosis-ferroptosis synergistic therapy. Appl Sci 2025; 15:10446.
27. Murakami H, Wang JL, Yu H. A novel ferroptosis-related microRNAs signature for predicting prognosis in endometrial cancer: An observational study. Medicine 2025; 104:e46102.
28. Saadh MJ, Ahmed HH, Sanghvi G, Isa MZB, Singh P, Kaur K, *et al.* Recent advances in the delivery of microRNAs via exosomes derived from MSCs, and their role in regulation of ferroptosis. Pathol Res Pract 2025; 270:155984.
29. Karam RA, Amer MM, Zidan HE. Long noncoding RNA NEAT1 expression and its target miR-124 in diabetic ischemic stroke patients. Genet Test Mol Biomarkers 2022; 26:398-407.
30. Wawrowski T, Surówka A, ZoBnierczuk M, Prowans P, Grabowska M, Kupnicka P, *et al.* The role of the SLC1A5 transporter on glutathione homeostasis and enterocyte apoptosis in chronic treatment of rats with immunosuppressive drugs. Int J Mol Sci 2025; 26:8330.
31. Yang XM, Yu H, Li JX, Li N, Li C, Xu DH, *et al.* Excitotoxic storms of ischemic stroke: a non-neuronal perspective. Mol Neurobiol 2024; 61:9562-9581.
32. Chen HN, Zang SH, Zhang RL, Chen PL, Wu SX. Association of anti-oxidant markers (Sod, Gsh, No, Catalase) with Ischemic stroke severity and recovery outcomes. J Med Biochem 2025; 44:895-904.
33. Chouinard VA, Feizi W, Chen X, Ren BY, Lewandowski KE, Anderson J, *et al.* Acute administration of intranasal insulin shows disrupted anti-oxidant response and glutathione (GSH) system measured by magnetic resonance spectroscopy in psychotic

disorders, compared to healthy participants. Biol Psychiatry 2025; 97:9:S11-S12.
34. Delgado-Martin S, Hugo M, Lopez-Rodriguez AB, de los Rios-salgado C, So PW, Martinez-Ruiz A. Role of the mitochondrial sodium/calcium exchanger NCLX in ferroptosis after ischemic stroke. Free Radic Biol Med 2025; 233:S47-S47.
35. Shi WJ, Yuan SH, Cheng GH, Zhang HL, Liu KJ, Ji XM, *et al.* Blood brain barrier-targeted lipid nanoparticles improved the neuroprotection of Ferrostatin-1 against cerebral ischemic damage in an experimental stroke model. Exp Neurol 2024; 379:114849.
36. Chen J, Deng XY, Lin T, Huang JF, Yang YS, Lian NF. Ferrostatin-1 reversed chronic intermittent hypoxia-induced ferroptosis in aortic endothelial cells via reprogramming mitochondrial function. Nat Sci Sleep 2024; 16:401-411.
37. Zhu DD, Wu SF, Li YF, Zhang Y, Chen JR, Ma JH, *et al.* Ferroptosis-related gene SLC1A5 is a novel prognostic biomarker and correlates with immune infiltrates in stomach adenocarcinoma. Cancer Cell Int 2022; 22:124.
38. Zhang MS, Zheng H, Jin H, Zhu XQ, Liu SW, Chen Y, *et al.* Regulating SLC7A11/GSH/GPX4 axis by glucose dyshomeostasis to simultaneously promote disulfidptosis, cuproptosis and ferroptosis. Bioact Mater 2025; 54:744-758.
39. Sangwan N, Singh J, Chauhan A, Prakash A, Khanduja KL, Medhi B, *et al.* Structure and dynamic simulation-based interactions of benzenoids, pyrroles and organooxygen compounds for effective targeting of GPX4 in ischemic stroke. J Biomol Struct Dyn 2023; 41:9143-9156.